A new user-friendly materials science end station at the FinEstBeAMS beamline of MAX IV

Journal of Physics: Conference Series **2380** (2022) 012048 doi:10.1088/1742-6596/2380/1/012048

A new user-friendly materials science end station at the FinEstBeAMS beamline of MAX IV

W Wang[1], A Kivimäki[1,2], K Chernenko[1], R Pärna[1,3], T Käämbre[3], E Kukk[4], K Kokko[4], M Valden[5], M Hirsimäki[5], M Kirm[3] and M Huttula[2]

[1]MAX IV Laboratory, Lund University, Sweden
[2]Nano and Molecular Systems Research Unit, University of Oulu, Finland
[3]Institute of Physics, University of Tartu, Estonia
[4]Department of Physics and Astronomy, University of Turku, Finland
[5]Faculty of Engineering and Natural Sciences, Tampere University, Finland

Abstract. FinEstBeAMS is an atmospheric and materials science beamline located at the 1.5 GeV storage ring of the MAX IV Laboratory in Lund, Sweden. It offers a very wide photon energy range 4.5-1300 eV and radiation with different polarization characteristics. The beamline has three end stations installed at two branch lines. The new solid state end station (SSES) is described in this paper. It is a high-throughput apparatus with flexible sample preparation options for X-ray photoemission, angle-resolved photoemission, and X-ray absorption spectroscopy. Three examples of experiments at room temperature demonstrate the capabilities of the SSES in the research field of surface science and condensed matter physics.

1. Introduction

FinEstBeAMS was funded and constructed in international collaboration between Finland and Estonia, and it has also received infrastructural support from MAX IV, a Swedish national laboratory. It is part of the MAX IV portfolio and open to all users similarly to any other beamline at the facility. FinEstBeAMS provides ultraviolet and soft X-ray radiation with precisely controlled and widely variable parameters [1,2]. The beamline has two branches: one is dedicated to ultra-high vacuum studies of surfaces and interfaces and the other, hosting two exchangeable end stations, to gas-phase experiments and photoluminescence in solids. Research performed at FinEstBeAMS extends from the electronic structure studies of free particles (atoms, molecules, clusters, and atmospheric aerosol particles) to formation analysis and nanoscale characterisation of surfaces and interfaces. The radiation source, an elliptically polarizing undulator (EPU), provides radiation with selectable polarization from linear (horizontal, vertical, or inclined direction) to circular (left and right). The photon energy range, covered with two gratings, starts from exceptionally low 4.5 eV and extends up to 1300 eV. The beamline has reached resolving power of 11000 at 400 eV photon energy using the exit slit of 10 μm in the monochromator. The smallest beam spot size achieved at the solid-state end station (SSES) is about 25 × 30 μm^2. The spot size's dependence on the exit slit size was reported in Ref. 2.

2. Experimental setup

FinEstBeAMS has three operational end stations: the gas-phase end station [3], the photoluminescence end station [4], and the solid-state end station. In this report, we will focus on the most recently

commissioned end station, the SSES. It has been designed as a high-throughput apparatus with flexible sample preparation options for X-ray photoemission (XPS), angle-resolved photoemission (ARPES), and X-ray absorption spectroscopy (XAS). The SSES is composed of four ultra-high vacuum (UHV) chambers connected by a distribution chamber, *i.e.*, an analysis chamber, a preparation chamber, a storage chamber, and a load-lock chamber (see Figure 1). The design of the system also allows sample transfer from a vacuum suitcase to the load lock and the preparation chamber. All the chambers can be pumped and vented independently. The main instrument is a SPECS PHOIBOS 150 R7 hemispherical electron analyser with a 2D delay line detector. The best kinetic energy resolution of the analyser is about 2 meV. The manipulator has 5-axis motorised motion, *i.e.*, three linear motions and two rotational motions (polar and azimuth). An open-cycle cryostat can be cooled using either liquid He or N_2. The preparation chamber is equipped with a low energy electron diffraction (LEED)/Auger setup and a quadrupole mass spectrometer. It is possible to quickly load, *e.g.*, an evaporation source or evaporation cell without venting the main preparation chamber through a pumping manifold.

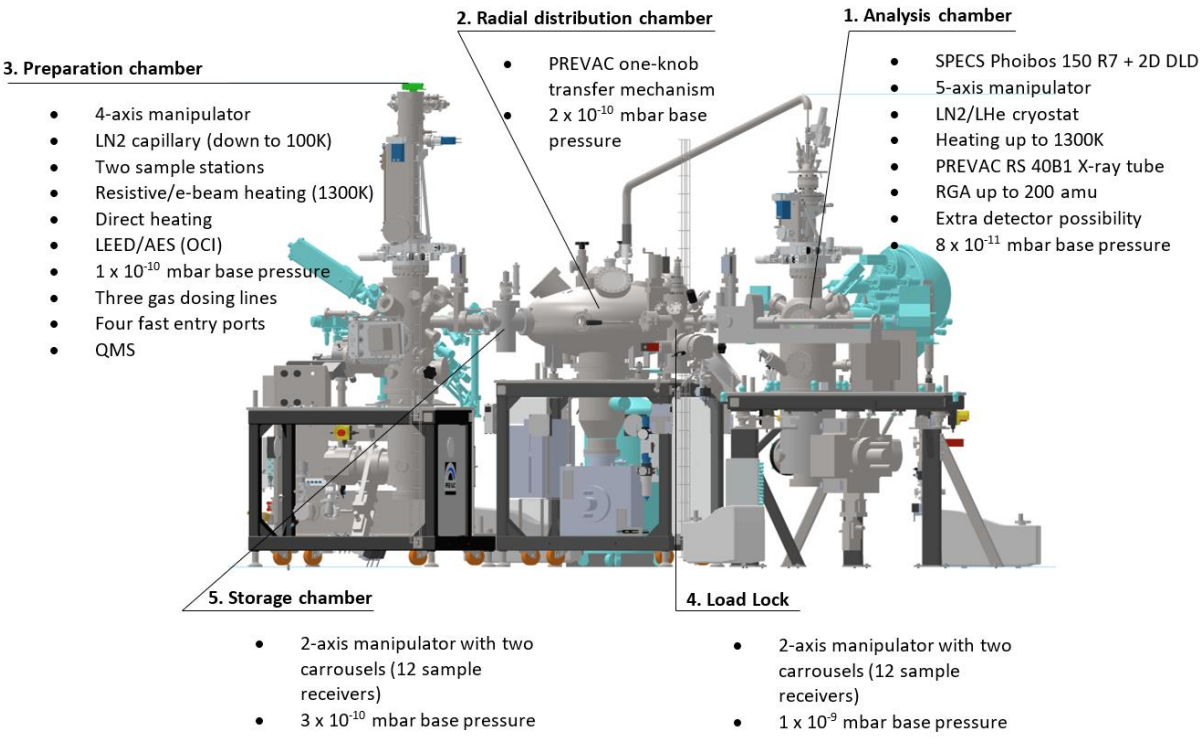

Figure 1. Schematic representation of the SSES with specifications of components and techniques in different UHV chambers.

3. Results and discussion

3.1. Au(111) single crystal

The first example is a study of the atomic and electronic band structure of a material's surface by LEED, core-level PES and ARPES. Au(111) single crystal is often used to commission a soft X-ray beamline because of its complicated but well-known atomic and electronic structure. It was cleaned by repeated cycles of sputtering with Ar^+ ions (1 keV) and annealing at approximately 400 ˚C. Figure 2(a) shows a typical LEED pattern of a herringbone superstructure of an atomically clean Au(111) surface. The size and orientation of the small hexagon around the (1×1) diffraction spot agrees with the "22 × √3" reconstruction [5,6]. The observation of two components in the Au 4f core level spectra corresponds to the location of Au atoms on the surface and in the bulk. By fitting the spectra with two pairs of peaks

described by Voigt functions, we extracted a binding energy shift of 0.34 eV between the surface and bulk components. Upon deconvolution of the Voigt function, the FWHM of the Lorentzian could indicate the intrinsic line width of the Au 4f level (the value of ~0.36 eV agrees with the literature value [7]), while the FWHM of the Gaussian simulates the combination of the instrumental resolution and interactions that the excited electron encountered during photoemission process. The Shockley surface state of the Au(111) was measured by ARPES. The bottom of the parabolic band locates at binding energy ~0.45 eV and the well resolved Rashba type of spin splitting is found with $\Delta k \approx 0.026$ Å^{-1}. These values agree with the previous experimental and calculated results [8,9].

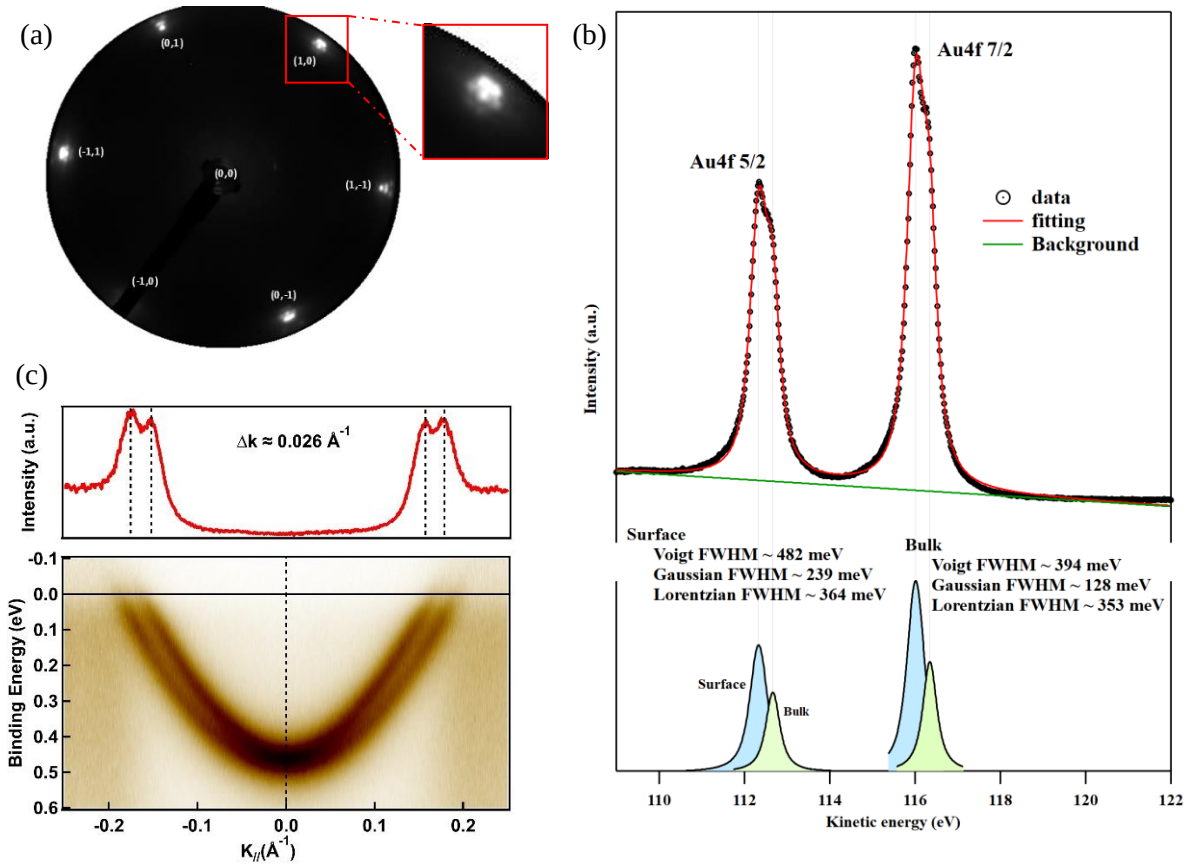

Figure 2. (a) LEED pattern (49 eV) from clean Au(111) single crystal surface. The zoomed parts in the red rectangle show details of the "22 × √3" superstructure diffraction around 1 × 1 spots; (b) Au 4f core level spectra obtained at 200 eV photon energy showing surface and bulk components with 0.34 eV binding energy shift; (c) ARPES (25 eV) of the Shockley surface state of Au(111) single crystal showing a well-resolved Rashba type of spin-split. The red line profile was extracted from the Fermi level with line width of 10 meV.

3.2. Graphene

The polarization of radiation plays an essential role in the study of the electronic chirality of quantum material. The second example is a study of the electronic chirality of a 1ML/2ML mixed graphene sample on 6H-SiC(0001), which was annealed to about 600 ˚C for 30 minutes by passing current through the sample. ARPES was measured at 22 eV excitation energy in order to observe the Dirac cone as close as possible to the condition where the photon beam hits the graphene surface at normal incidence. Four polarization configurations were employed: linear horizontal (LHP), linear vertical (LVP), linear

inclined (IP), and circular polarization (CP). The polarization degree was better than 99% for LHP and LVP, and better than 95% for IP and CP.

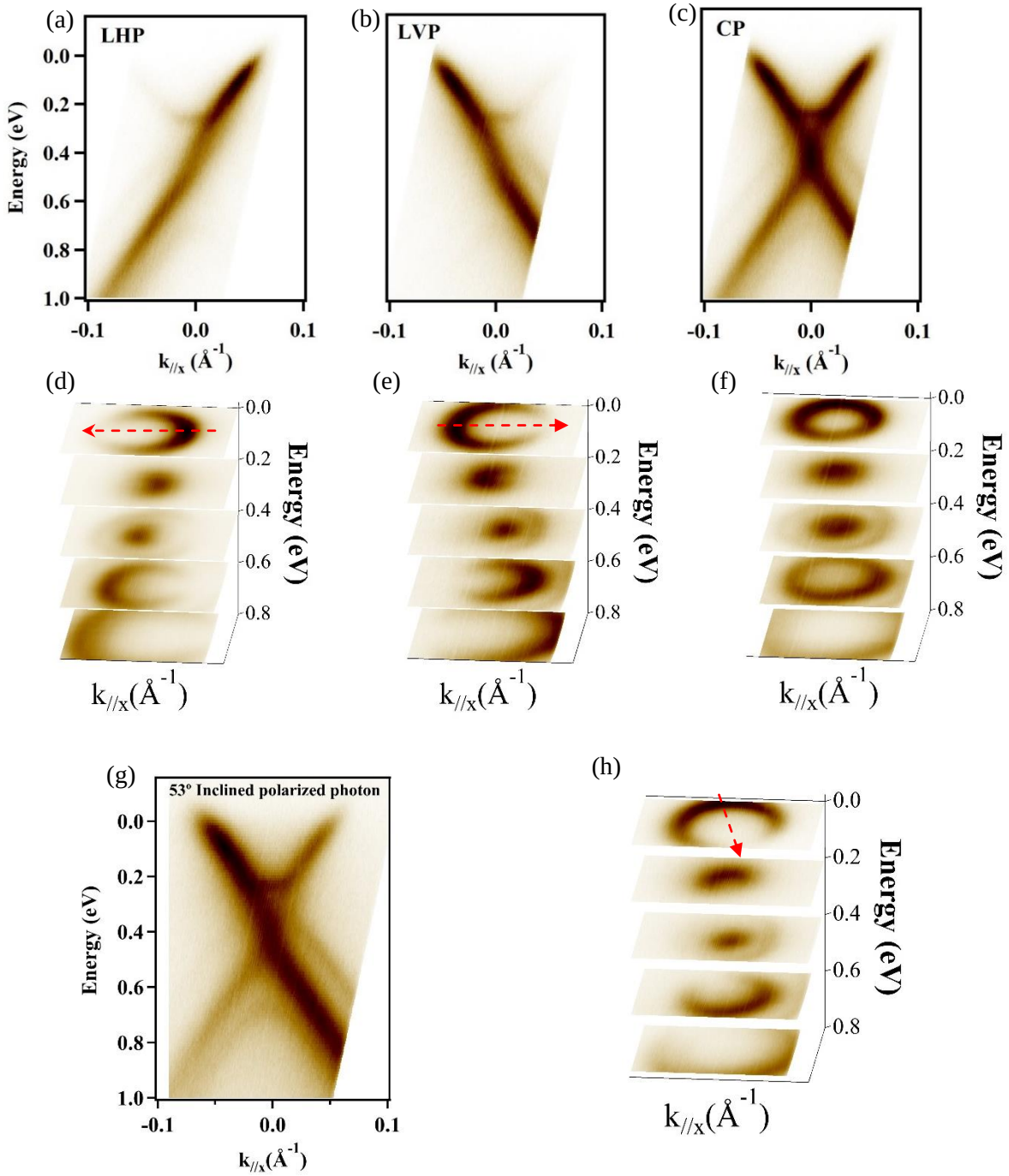

Figure 3. Panels (a-c) and (g) show ARPES results obtained on a mixed monolayer-bilayer graphene sample. The data were taken along the $\bar{\Gamma}\bar{K}$ direction in the surface Brillouin zone of graphene. The $\bar{K}$ point is set as a reference "0" in the momentum space ($k_{//x}$). The spectra were measured using LHP, LVP, CP and IP respectively. In panels (d-f) and (h), the 3D plot of constant energy contours show the polarization dependence of the 'dark corridor' of the Dirac cone. Red arrows indicate the orientation of the dark corridor.

There are two carbon atoms in the honeycomb lattice of graphene, which leads to two bands originating from the two triangular sublattices. The charge carriers in these two bands accumulate a Berry phase on closed-loop paths resulting in the absence of backscattering [10]. The effect is observed in ARPES experiments on graphene with linearly polarized light, showing suppression of the photoemission intensity on part of the Fermi surface, a so-called 'dark' corridor. In the literature, researchers have shown that it is possible to rotate the corridor by changing polarization from LHP to LVP and CP [11,12]. The data set in figure 3 shows that the orientation of the 'dark corridor' is rotated by 90˚ and 180˚ upon switching from LHP to CP and LVP, respectively. Note that the dark corridor is partially illuminated by CP, which disagrees with the results and conclusions of Ref. 12. To our best knowledge, the full illumination of graphene's dark corridor has not been achieved experimentally by circularly polarized light. Our observation reopens the discussion about the origin of the suppression of the photoemission intensity in the graphene π band. In addition, thanks to the flexibility of our EPU, we could probe for the first time the dark corridor with inclined linearly polarized light. Figure 3(h) shows that the dark corridor rotates about 110˚ with respect to figure 3 (d) by using polarized light inclined with about 55˚ (54.7˚ is the 'magic angle' [13]). The rotating ratio between inclined polarization angle and dark corridor orientation is 2, which is consistent with the case that LVP is 90˚ inclined respect to LHP resulting in the dark corridor's rotation by 180˚. In the near future, we will be able to freely select any angle of inclined polarized light to investigate the origin of the dark corridor more comprehensively. Last but not least, the observation of the flat band close to the Dirac point is another reason why users could come to perform ARPES measurement at the SSES. As mentioned in Ref. 14, such a flat band has been observed many times before but ignored because the resolution was not sufficient to reveal the details of the band dispersion. Evidently, the performance of the SSES and FinEstBeAMS beamline could provide users with good data about these competitive research topics.

3.3. XAS at 3d transition metal 2p edge: α-Fe_2O_3

The third example evaluates the signal and stability levels in the energy region of the 2p core absorption edges of 3d transition metal, which are at considerably higher photon energies than discussed so far. For that purpose, we chose hematite (α -Fe_2O_3, powder sample pressed in indium) as an appropriate test sample, since it is very stable both during extended storage and under soft X-ray illumination, it has sharp features, which are relatively well modelled already on the crystal field multiple level [15], and it has been extensively studied ([16] and references therein).

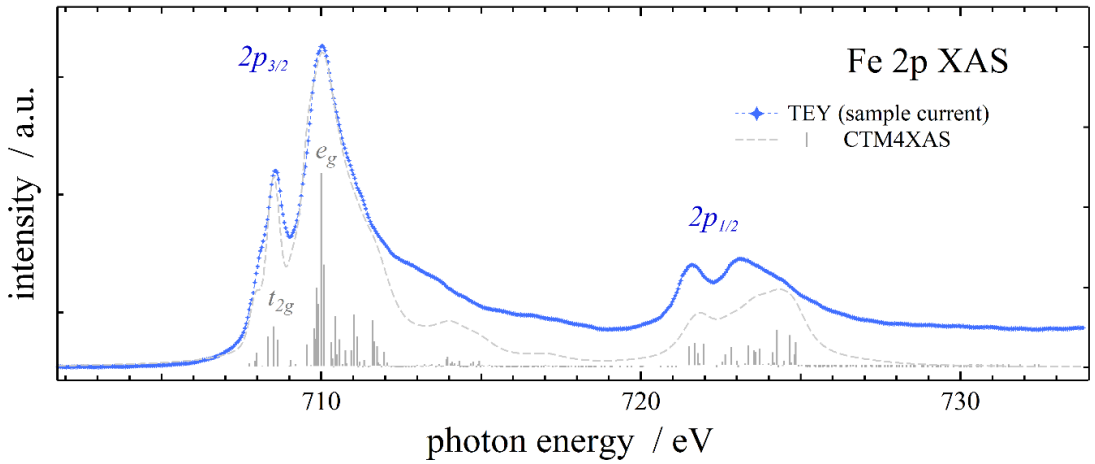

Figure 4. Fe 2p-3d photoabsorption scan from a hematite sample, recorded in total electron yield mode by measuring the sample drain current (symbols). The grey sticks (transitions) and line (envelope) give a crystal field split final state multiples of 2p-3d transitions for Fe3+ in 10Dq=1.2 eV octahedral crystal field.

Figure 4 displays the Fe 2p XAS of hematite recorded in total electron yield (TEY) mode, by measuring sample drain current using a picoammeter [16]. (Partial electron yield by collecting Auger electrons with the electron analyser is also available at the SSES.) Our result, recorded using a 30 μm monochromator slit is in line with literature reported (and not resolution limited) spectra [17], showing even a weak elbow below the first ($2p_{3/2}$, t_{2g}) peak, which is also reproduced in the calculated curve. The time per absorption scan is presently relatively long (about 20 minutes for the curve in Fig. 4) because of the dead times involved in setting stepwise both the undulator gap and photon energy. It can be shortened considerably in the near future when the measurement of absorption scans in constant speed monochromator mode becomes available. Another impending technical improvement that regards XAS scans is the introduction of a gold mesh after the last optical element for the measurement of the reference current. That will improve normalization of the XAS spectra particularly at the O 1s and C 1s edges.

4. Acknowledgement

Staff of the MAX IV Laboratory are gratefully acknowledged for assistance during design, construction, commissioning and operation of the FinEstBeAMS beamline. Financial support was provided by European Regional Development Fund (grant No. TK-141 HiTechDevices 2014-2020.4.01.15-0011 to University of Tartu; grant No. MAX-TEENUS 2014-2020.4.01.20-0278 to University of Tartu); Estonian Research Council (grant No. FinEstBeAMS TT-20 to University of Tartu, grant No. PRG-629 to University of Tartu); Jane & Aatos Erkko Foundation (grant No. SOFUS); Business Finland (grant No. 1464/31/2019); Academy of Finland (grant No. 319042; grant No. 326461; grant No. 326406; grant No. 320165); University of Oulu; University of Turku; Tampere University; University of Tartu; the Swedish Research council under contract 2018-07152, the Swedish Governmental Agency for Innovation Systems under contract 2018-04969, and Formas under contract 2019-02496.

References

[1] Pärna R *et al* 2017 *Nucl. Instrum. Methods Phys. Res. A* **859** 83
[2] Chernenko K *et al* 2021 *J. Synchrotron Rad.* **28** 1620
[3] Kooser K, Kivimäki A, Turunen P, Pärna R, Reisberg L, Kirm M, Valden M, Huttula M and Kukk E 2020 *J. Synchrotron Rad.* **27** 1080
[4] Pankratov V *et al* 2019 *Radiat. Meas.* **121** 91
[5] Huang K G, Gibbs D, Zehner D M, Sandy A R and Mochrie S G J 1990 *Phys. Rev. Lett.* **65** 3313
[6] Hanke F and Björk J 2013 *Phys. Rev. B* **87** 235422
[7] Heimann P, van der Veen J F and Eastman D E 1981 *Solid State Commun.* **38** 595
[8] Henk J, Hoesch M, Osterwalder J, Ernst A and Bruno P 2004 *J. Phys. Condens. Matter* **16** 7581
[9] Tusche C, Krasyuk A and Kirschner J 2015 *Ultramicroscopy* **159** 520
[10] Bliokh K Y 2005 *Phys. Lett. A* **344** 127
[11] Gierz I, Henk J, Hochst H, Ast C R and Kern K 2011 *Phys. Rev. B* **83** 121408(R)
[12] Liu Y, Bian G, Miller T and Chiang T-C 2011 *Phys. Rev. Lett.* **107** 166803
[13] Erickson S J, Prost R W and Timins M E 1993 *Radiology* **188** 23
[14] Marchenko D, Evtushinsky D V, Golias E, Varykhalov A, Seyller Th, Rader O 2018 *Sci. Adv.* **4** 0059
[15] Stavitski E and de Groot M F F 2010 *Micron* **41** 687
[16] Avila-Abellan J et al 2017 *Proceedings of the 16th International Conference on Accelerator and Large Experimental Control Systems* p. 137
[17] Miedema P S and de Groot M F F 2013 *J. Electron Spectr. Relat. Phenom.* **187** 32